1995ApJ...452..613C

THE ASTROPHYSICAL JOURNAL, 452:613–626, 1995 October 20

SPECTRAL EVIDENCE FOR SHOCK-IONIZED GAS ALONG THE JETS OF NGC 4258

GERALD CECIL,[1] JON A. MORSE,[2] AND SYLVAIN VEILLEUX[3,4,5]

Received 1995 February 15; accepted 1995 May 5

ABSTRACT

We use Fabry-Perot and long-slit spectra with radio, molecular, and X-ray data sets to study the twisted, multistrand jets in the nearby active galaxy NGC 4258 (M106). Their several arcminute extent and the extensive wavelength coverage of their interaction with the ISM make these jets an important laboratory for studying the processes likely to dominate the appearance of high-z radio galaxies. A VLA A-array image at 20 cm traces the jet down to 2″ (70 pc) radius and shows that it is perpendicular to the subparsec nuclear disk that is delineated by H_2O masers. Our long-slit spectra span the jet and range over 3640–8560 Å at 4.5 Å resolution. We measure a central stellar velocity dispersion of 171 km s^{-1}. This is smaller than the line widths of the ionized gas and is too low to explain the observed oscillations in the centroids of the emission-line profiles by virial motion within the bulge potential. Mean stellar velocities agree with those of the gas along the jet axis and are consistent with bar-forced motions in the large-scale disk of the galaxy. From the emission-line flux ratios, we find LINER-like gaseous excitation along the jets and constrain the gas temperatures. For the N^+ and O^+ emitting gas, we found that $T < 10^4$ K, and for the S^+ gas $T < 19{,}000$ K. The O^{++} temperature is weakly constrained to be less than 30,000 K. Flux ratios remain constant along the SE jet, with ionization parameter $\log U \approx -3.5$. Our models show that these ratios can be generated by $\approx$350 km s^{-1} shocks, velocities consistent with the amplitude of kinematic oscillations in the emission-line profiles and with the observed thermal X-ray spectrum of the jet of temperature 0.3 keV. A modest ambient gas density of 0.2 cm^{-3} can produce both the jet's X-ray flux and enough ionizing photons to account for the jet's Hα flux. In contrast, the present ionizing flux from the AGN is $\approx 10^3$ times too low to directly photoionize the jets. Therefore, molecular gas that is known to lie along the jets may be shocked and photoionized locally as it is entrained. We constrain the star formation induced by the SE jet. The jets do not emit a continuum within the interval $\lambda\lambda = 0.38$–0.88 μm down to a surface brightness of 3×10^{-17} ergs cm^{-2} s^{-1} $Å^{-1}$ $arcsec^{-2}$.

Subject headings: galaxies: individual (NGC 4258) — galaxies: jets — shock waves — X-rays: galaxies

1. INTRODUCTION

The multistrand jets of NGC 4258 have been studied across the electromagnetic spectrum. The unparalleled large spatial extent of these jets (2′.5 in line emission, 5′ in the radio continuum and X-rays), their strong interaction with the interstellar medium (ISM) of this galaxy, and the apparent profound influence of these gaseous processes on the structure of high-z radio galaxies (see, e.g., McCarthy 1993) make NGC 4258 an important laboratory for studying the uncertain dynamical state of gas that is influenced by an astrophysical jet. In this paper we study the source of gaseous excitation along the jets. We combine Fabry-Perot area spectrophotometry of the [O III] λ5007 line with long-slit spectra taken along the jet, and galaxy major axis. The [O III] data are used with spectra from Cecil, Wilson, & Tully (1992, hereafter CWT) to constrain the spatiokinematic variations of the [O III]/Hα and [N II]/Hα flux ratios. The long-slit spectra have sufficient resolution (4.5 Å FWHM) to see the major trends in the complex gas motions (studied in detail with the few-line area spectrophotometry of CWT). They also span the wavelength range 3640–8560 Å to constrain line ratios that are diagnostic of temperatures and the excitation of the ionized gas along the jets.

Discovered by their Hα emission (Courtès & Cruvellier 1961), the full extent of the jets was revealed in the radio continuum (van der Kruit, Oort, & Mathewson 1972). Visual emission-line spectra (van der Kruit 1974) showed that most of the gas is not radiatively excited by hot stars. The spectra also showed that ionized gas near the jets does not follow normal galactic rotation. The H I velocity field at 23″ FWHM resolution (van Albada 1980) is consistent with motions expected for bar streaming rather than direct agitation by the jets. Higher resolution Hα images (Ford et al. 1986) showed that within 40″ radius the jets are multistrand entities and suggested that the strands wrap around one another. In higher resolution radio continuum images (van Albada & van der Hulst 1982), the filamentary nature of the jets is apparent in this region, but resolution attained to date is still too low to separate the individual strands.

More recently, CO interferometric images have highlighted interactions between the jets and ambient molecular gas (Martin et al. 1989; Plante et al. 1991; Krause et al. 1990; Plante, Handa, & Lo 1994). The interaction is striking, both spatially and kinematically, in the Fabry-Perot [N II] λ6583 and Hα spectral grids (or "data cubes") that we discussed in CWT. We isolated the interacting jets from the overall bar-forced gas motions in the disk. We showed that the prominent zigzag oscillations of amplitude ±325 km s^{-1} within 25″

---

[1] Department of Physics and Astronomy, University of North Carolina, CB No. 3255, Chapel Hill, NC 27599-3255.

[2] Space Telescope Science Institute, Baltimore, MD 21218.

[3] Kitt Peak National Observatory, NOAO, P.O. Box 26732, Tucson, AZ 85726-6732.

[4] Present address: University of Maryland, Department of Astronomy, College Park, MD 20742.

[5] Hubble Fellow.

radius SE of the nucleus (Rubin & Graham 1990) are correlated with the spatial oscillations visible in the Hα image of Ford et al. (1986). Based on this correlation, we suggested that the ionized gas is organized into helices. However, our spatial and spectral resolutions were insufficient to distinguish between true helical motion and ballistic expansion from oscillating sources.

The observed gas velocities imply postshock temperatures above 10^6 K. Dutil, Beauchamp, & Roy (1995) have presented a 0.53–0.70 μm color map (made with filters that exclude prominent emission lines) that shows a "green" extension to 15″ radius along P.A. 147° that is 6″ wide. They argue that this is free-free emission behind a high-velocity shock. In Cecil, Wilson, & De Pree (1995, hereafter CWD), we reported that the *ROSAT* HRI image of NGC 4258 shows that the X-ray emission is tightly concentrated along the jets, while the multiband PSPC detector shows that this gas has a thermal spectrum with $kT = 0.3 \pm 0.05$ keV. We argued in CWD that this gas has been shocked by motions of ≈500 km s^{-1} as it was entrained from the adjacent molecular clouds (Krause et al. 1990; Plante et al. 1994). Such shock velocities are more consistent with the observed kinematic wiggles along the jet if the intrinsic flow is along helical rather than linear (ballistic) paths, because in the former much of the motion would occasionally project along the line of sight. In contrast, the ballistic flow less favored in CWT would be expected to remain largely perpendicular to the line of sight. It would have much larger velocities, hence postshock X-ray temperatures, than we observe.

Despite these extensive multifrequency data, no comprehensive study of the visual spectrum of the jets has been undertaken since van der Kruit (1974) published a dozen long-slit, image-tube spectra that he had acquired across the galaxy with the Palomar 5 m telescope. Because he also sought to study the overall disk motion, he did not place all of his slits across the jets. Emission-line flux ratios were poorly constrained because of the limited dynamic range of his photographic spectra.

Now that the disk motion has been thoroughly mapped by visual emission-line area spectrophotometry (CWT), it is appropriate to refocus attention on the emission-line spectrum of the jets and on the circumnuclear stellar motions. The jets are sufficiently linear, at least in their X-ray emission (CWD), that they can be intersected at several points with a single long slit. Two previous studies have discussed the gaseous excitation. Dettmar & Koribalski (1990) have discussed a red CCD spectrum taken along the jets, and they confirm the unusual excitation patterns first noted by van der Kruit (1974). Although mostly concerned with the nucleus, Stüwe, Schulz, & Hühnermann (1992) did discuss the gaseous excitation within 10″ radius, based on spectra obtained along five position angles.

These spectral studies all concentrated on the brightest visual emission lines. However, the great improvements in detector sensitivity since van der Kruit's image-tube measurements have now allowed us to place useful constraints on the fainter emission lines that are diagnostic of physical conditions in the ionized gas. In § 2, we outline our observations and discuss the reduction of our various data sets. In § 3, physical parameters of the gas are derived from our spectra. In § 4 we compare our data to the predictions of published photoionization and new shock models. We assume a distance of 6.5 Mpc to NGC 4258. We summarize our main results in § 5.

2. OBSERVATIONS AND DATA REDUCTION

2.1. *Imaging Spectrophotometry*

Table 1 summarizes our spectral and imaging data. To compare the kinematics of higher excitation gas to those of Hα, the Hawaii Imaging Fabry-Perot Interferometer (HIFI; Bland & Tully 1989) was used during the nights of 1992 March 15–16 at the Cassegrain focus of the University of Hawaii 2.2 m telescope to produce a complete grid of [O III] λ5007 emission-line profiles across the southeast half of NGC 4258. These spectra were recorded with a low-noise (5 e^- rms readout; however, see below) 1024^2 pixel Tektronix CCD in photometric conditions, with average seeing ∼1″ FWHM, and a pixel scale of 0″.84. A finesse 60 etalon with free spectral range 67 Å at [O III] yielded a velocity resolution of 70 km s^{-1} (Nyquist sampling). A filter with flat-topped transmission profile centered at 5023 and 50 Å FWHM bandwidth passed only one etalon order, so fluxed emission-line profiles could be synthesized. Our 41 10 minute exposures (velocity slices) spanned ±600 km s^{-1} around the systemic velocity of the galaxy. We took the images at random wavelengths within this range to minimize the influence of systematics that depend on time. The etalon optical gap was flushed with dry nitrogen gas to minimize pressure and humidity changes.

On the first night an intermittent failure of the dome rotation caused the dome slit to lag behind the telescope, so partially occulting up to 30% of the light beam. This was discovered after several hours, whereupon photometry was recovered by reobserving several wavelengths where light had been attenuated.

Instrumental stability was monitored by periodically imaging a diffused neon lamp at a nominally constant etalon gap spacing. A constant ring center showed that no shifts occurred in the etalon optical axis, while a constant ring radius showed that variations in pressure and humidity had not

TABLE 1

Summary of Observations

Date	Instrument/Telescope	Object	Exposure (s)	Spectral Range (Å)
1992 Mar 15–16......	Fabry-Perot/UH 2.2 m	NGC 4258	41 × 600	λ5007+($V_{\mathrm{sys}} \pm 600$) km s^{-1}
1993 May 26	CCD Direct/KPNO 0.9 m	NGC 4258	1200	*U* band
1993 Jun 11...........	Goldcam/KPNO 2.1 m	NGC 4258	3 × 1800	3640–6200
1993 Jun 13...........	Goldcam/KPNO 2.1 m	NGC 4258	4 × 3000	4500–7000
1994 Apr 7............	Goldcam/KPNO 2.1 m	NGC 4258	2 × 3000	6150–8940
1994 Apr 7............	Goldcam/KPNO 2.1 m	NGC 3115	1200	3650–6300
1994 Apr 7............	Goldcam/KPNO 2.1 m	NGC 3115	1200	6150–8940

altered the optical gap and capacitance micrometry, respectively. Several bright sky lines were also used during the data reduction to check stability. At the beginning and end of the night, series of exposures were made of the neon lamp and of a current-stabilized continuum lamp for wavelength calibration and flat-fielding purposes, respectively. The flat-field exposures were obtained at the same etalon gaps as the data. To provide an absolute flux calibration, photometric standard stars were observed with the same setup.

The data were reduced into spectral grids using our standard procedure (Cecil, Bland, & Tully 1990). The limit on the minimum attainable flux was set by a visible 60 Hz pickup from the dome environment that was described by remote technical support as "part of the readout." Attempts to remove this contaminant with a software notch filter were unsuccessful because its phase jittered. Cosmic rays were removed by median filtering each spectrum above an empirically determined threshold and with the added condition that the candidate anomalies be spikes in only one velocity channel. The intensity of each frame was scaled appropriately to correct for mean Mauna Kea extinction at the mid-exposure airmass. Then the data were phase calibrated using the theoretical phase curve (see Bland & Tully 1989) and fits to lamp lines in the calibration cube. Next, the spectra were placed on an absolute flux scale by comparing the raw counts from photometric standard stars with the absolute fluxes tabulated in Stone (1977) for Feige 34 and Goodrich & Veilleux (1988) for θ Vir. Our fluxing procedure is detailed in Bland-Hawthorn, Shopbell, & Veilleux (1995).

To derive gaseous kinematics and line fluxes of O^{++} across the SE jet, the ~10,000 Fabry-Perot spectra were then fitted with single Gaussians and a variable flat continuum These fits show that the gas motions in [O III] are similar on average across the jet to those mapped in [N II] and Hα. To verify that the dome problem mentioned above had been fully corrected for, the [O III] λ5007 fluxes were cross-checked against those from our long-slit spectrum (§ 2.3) by simulating the long slit in our data cube. Together, these photometric observations revealed the error reported in CWD in the Hα fluxes that were tabulated in CWT. (The values reported by Stüwe et al. (1992) had also aroused our suspicion that the CWT fluxes were too low.) Finally, we used average reddening values derived along our final long-slit spectrum (§ 2.3) to deredden the [O III], [N II], and Hα line fluxes in our data cubes of the SE jet.

Figure 1 (Plate 16) shows images of the flux sums and the [O III]/Hα line ratios. In the [N II] and Hα lines all three jet strands have similar brightnesses. The most obvious difference between these lines and [O III] is the enhanced prominence of the southernmost strand of the SE jet in the higher excitation line compared to the other strands. In fact, this strand coincides with the jet as it appears in the 6 cm VLA[6] image discussed in CWD, and its bright end at the bottom of panel *c* has an analog in the *ROSAT* HRI X-ray image (Fig. 5 of CWD). This supports the conjecture of Martin et al. (1989) that it is the currently active strand of the jet.

2.2. *U-Band CCD Image*

On 1993 May 26, J. Rose used a thinned 2048^2 Tektronix CCD (T2KA) to take a 1200 s *U*-band exposure of NGC 4258 at the KPNO 0.9 m telescope. He kindly made these data available to us to address the long-standing uncertainty on the *U*-band visibility of the jets. The image was calibrated by observations of Hayes standard stars. A master flat image was assembled from twilight sky exposures. Standard IRAF[7] tasks were used for bias subtraction and flat-fielding. Prominent cosmic rays were removed with the "cosmic" task; the "imedit" task was used to remove the rest.

Figure 2 (Plate 17) confirms that the SE jet is quite prominent across its entire width while the NW jet is detected faintly. However, the spectra discussed in the next section show that this arises because of the strong [O II]λ3727 emission of the jets.

2.3. *Long-Slit Spectrophotometry*

2.3.1. *Observations and Basic Reductions*

Long-slit spectra were obtained with the Goldcam CCD spectrograph at the Cassegrain focus of the KPNO 2.1 m telescope, on the evenings of 1993 June 11 and 13 and by service observations during the evening of 1994 April 7. These spectra complement the Fabry-Perot data by extending the wavelength coverage to constrain other line diagnostics. We used the "26new" grating with 600 grooves mm^{-1} in first order and a 2″ wide slit to provide a spectral resolution of 4.4 Å FWHM. Most spectra were obtained in 1″.3–2″ seeing, and through thin cirrus in 1994. The detectors, Loral 3072 × 1024 15 μm pixel CCDs (read noise ~15 e^- rms), provided a spatial scale of 0″.78 pixel^{-1}.

CWD showed that the peak X-ray flux is almost linear along P.A. −30°, the major axis of the galaxy, so we placed the slit through the nucleus at this angle. This was not the parallactic angle, so differential atmospheric refraction altered slightly the positions on the galaxy that were sampled at different wavelengths; the shift, at its worst in the blue, is less than the width of the slit. In addition, ionized gas associated with the SE jet is almost 9″ wide, and our slit obviously does not follow the twisting strands. Therefore, the spectra yield average excitation conditions along the SE jet, in the region coextensive with the brightest X-ray emission. Indeed, our Fabry-Perot data cubes map the full spatial extent of the gaseous excitation in two important flux ratios and show (Fig. 1*d*) occasional twofold increases above the slit values at points off our slit.

Because the ends of this long chip are not imaged in sharp focus, we used only the middle 2000 pixels in the dispersed direction. We made projector flat-field exposures at the same orientations of the telescope as for our galaxy spectra to successfully divide out the strong interference fringing longward of 0.7 μm (peak-to-peak amplitude up to 20%). Spectra of the internal projector lamp, the twilight sky and a He-Ne-Ar comparison lamp were obtained for flat-fielding, slit illumination, and wavelength calibration purposes, respectively. The secondary standard star Feige 34 served as an absolute flux calibrator.

Standard IRAF SPECRED procedures were used to produce wavelength calibrated and fluxed long-slit spectra. The spectra were linearized with fourth-order Chebyshev polynomials, which were constrained typically by 65 emission arc lines. Fit residuals to the arcs were $\lesssim 0.05$ Å for all spectra.

---

[6] The VLA is a facility of the National Radio Astronomy Observatory, which is operated by Associated Universities, Inc., under contract with the National Science Foundation.

[7] IRAF is distributed by the National Optical Astronomy Observatory which is operated by the Association of Universities for Research in Astronomy, Inc., under contract to the National Science Foundation.

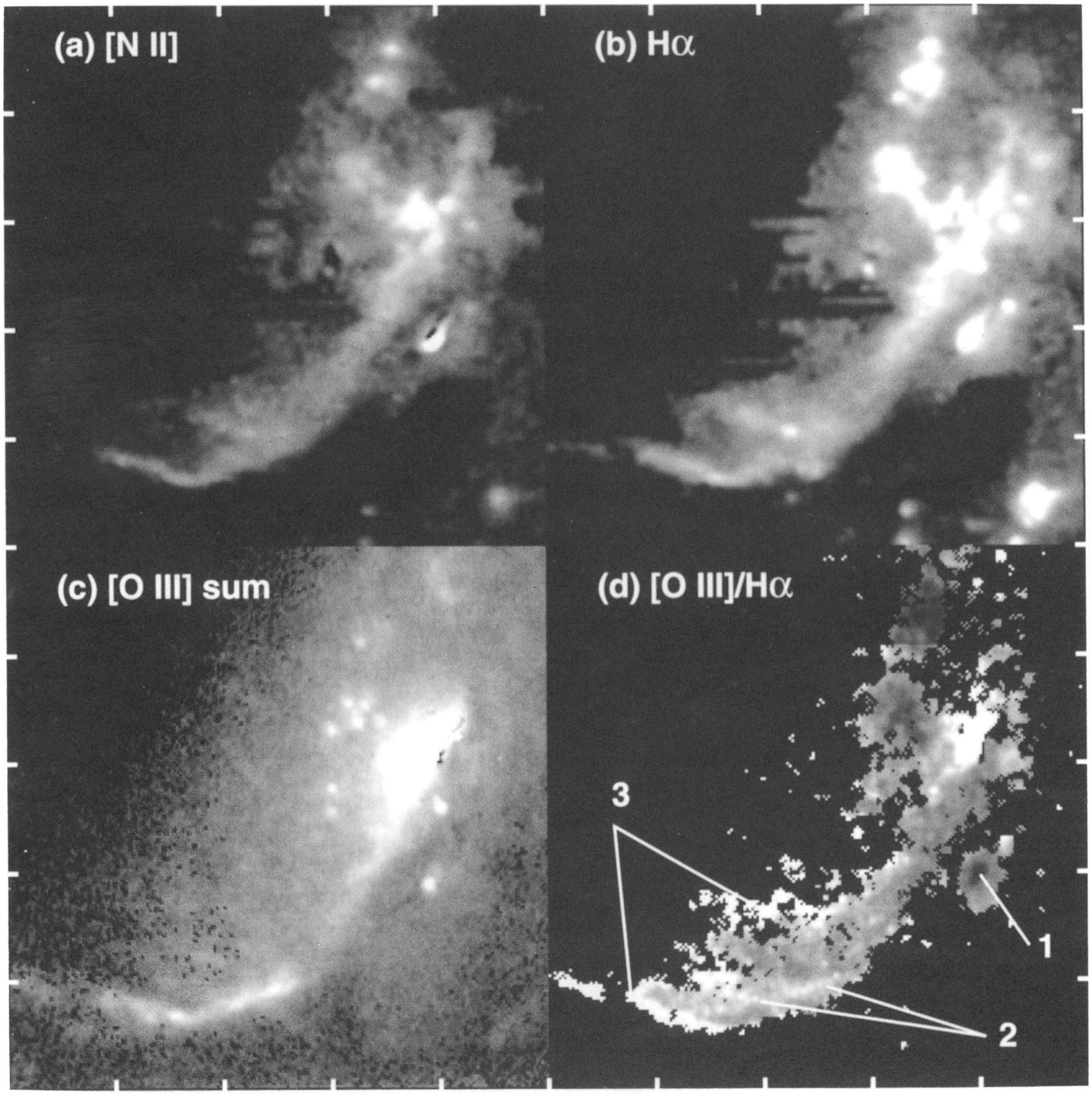

FIG. 1.—Continuum-subtracted emission-line images and their ratio [O III]/Hα along the SE jet. Ticks are at 33″ intervals; N is at top, and E is at left. In panels *a–b*, the line flux has been established from Gaussian fits to an emission-line profile at each point plotted; the fitted continuum level has been subtracted. Panel *c* is the sum of [O III] monochromatic images that spans the SE jet. In the ratio image, panel *d*, bright means high excitation. The gray scale is linear, with ratios ranging from 0.1 to 1.9 (*white*). The Hα and [N II] λ6583 images are from CWT, where the [N II] λ6583/Hα ratio image is also shown. The three strands of the SE jet are equally prominent in Hα (and [N II]; see CWT), but one strand dominates in the [O III] and ratio images (point No. 2). Point No.1 has low excitation and coincides with the end of the linear radio jet. The trailing strands (points No. 3) have high excitation, as does the region near the nucleus.

CECIL, MORSE, & VEILLEUX (see 452, 615)

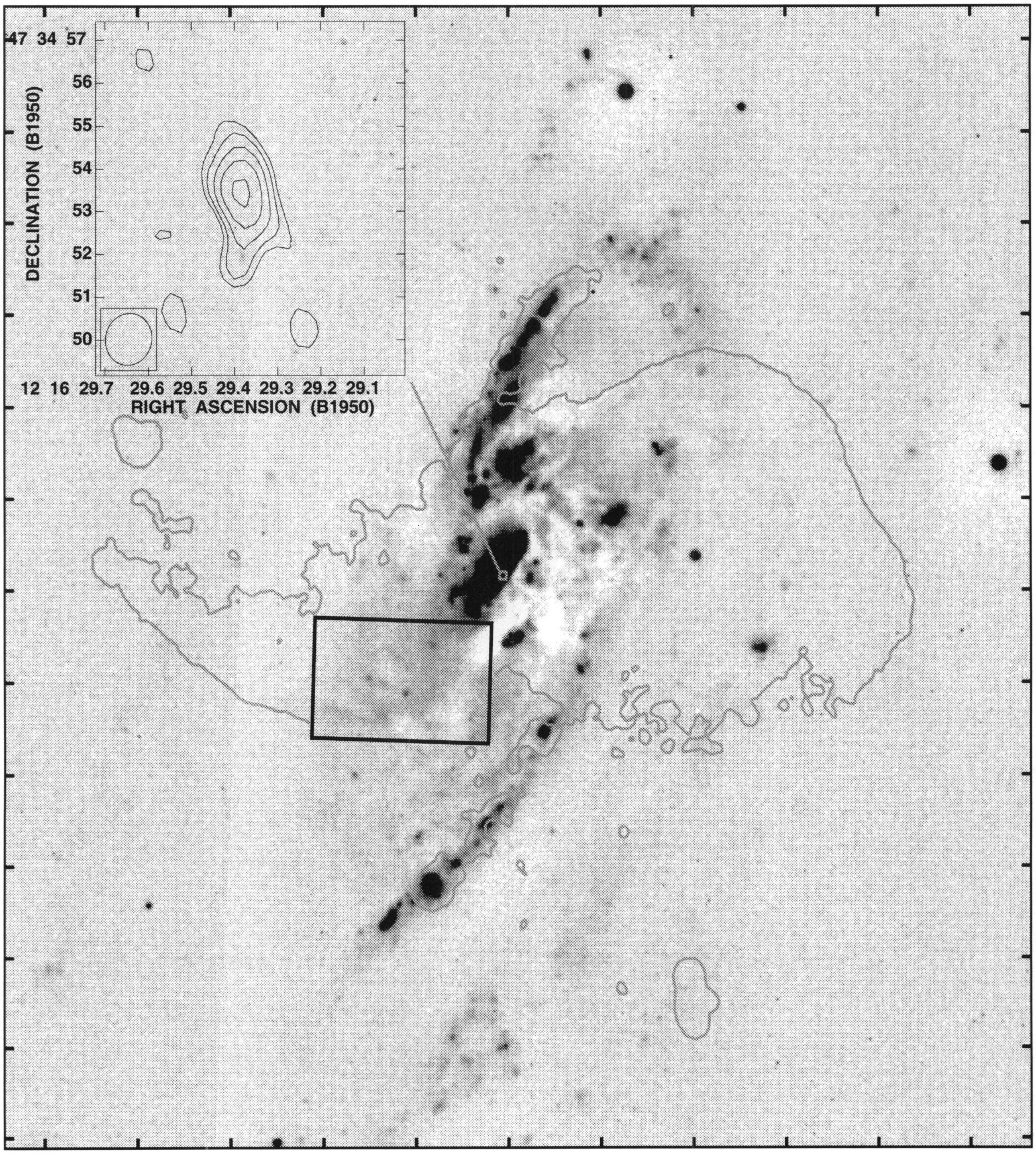

FIG. 2.—*U*-band CCD image from the KPNO 0.9 m telescope, shown in inverted gray scale. Ticks at 1′ intervals; N is at top, and E is at left. The 20 cm multiconfiguration VLA image briefly discussed in CWT is contoured to show the extent of the jets. Our long-slit spectrum along the major axis shows (P.A. −30°) that the multipronged SE jet is visible within the black box on this image because of its strong [O II] λ3727 emission. The NW jet strands are much more prominent in the radio than in the *U* image. The insert contours in black the near-nuclear flux as measured in a 35 minute exposure from the VLA archive, at 20 cm with the A-array; note the scale change relative to the main figure. Some beam smearing is evident along P.A. 30° in the radio image, which was centered on supernova 1981K ≈ 30″ NNE of the nucleus. However, the extension along P.A. 170° is real and is perpendicular to the disk of H_2O masers mapped by Miyoshi et al. (1995).

CECIL, MORSE, & VEILLEUX (see 452, 615)

The multiple blue exposures were combined with the AVSIGCLIP option to remove cosmic rays. For the blue spectra obtained in 1993, it was possible to approximate the sky emission-line spectrum with the light from the slit ends. However, in the red spectrum obtained in 1994, starlight is detected along the full length of the slit. So, the sky spectrum was established from a separate blank field exposure of 1200 s taken between the two red spectra of NGC 4258. To decrease noise, at each wavelength of this spectrum all intensities along the slit were fitted with a Chebyshev polynomial of third order which was then summed and subtracted from the galaxy spectrum. Following sky subtraction, all of the galaxy spectra were combined into a single composite image, whose wavelength scale was logarithmically rebinned into intervals of 100 km s^{-1}.

2.3.2. *Starlight Subtraction and Estimation of Stellar Kinematics*

It was then necessary to subtract the underlying starlight in this image to determine accurately the intensity of spectral lines, including that of Hα, which is affected by Balmer absorption near the nucleus. We also wished to search for spectral evidence of the "green" elongation that Dutil et al. (1995) showed in their 0.53–0.70 μm color map.

Inspection showed that the nuclear spectrum of the S0 galaxy NGC 3115 is a good match to the circumnuclear metal absorption lines of NGC 4258. Therefore, during the 1994 run, blue and red spectra were obtained of NGC 3115 with the same instrument setup. To establish stellar recessional velocities and velocity dispersions of both galaxies, the IRAF "fitprofs" task was used to fit simultaneously the IR Ca absorption triplet with Gaussians of the same width and a single velocity shift. Comparing the derived widths, we next smoothed each row of the NGC 4258 spectrum with a Gaussian function to match the stellar velocity dispersion of the NGC 3115 template. Then we used the IRAF "fxcor" task to find the cross-correlation lag of each spectrum of NGC 4258 relative to that of the template. By lagging the template and scaling its intensity, we removed most of the metal lines from each row of the NGC 4258 spectrum and mapped stellar motions out to radii of 20″ SE of the nucleus and 30″ NW. Figure 3 shows the spectrum before and after this procedure.

The IRAF programs do not return useful estimates of the velocity dispersion. We therefore convolved our spectra of the radial velocity standard star HD 101013 with Gaussians of different width. Best agreement with the observed widths of the Ca triplet in the nuclear pixel of NGC 4258 was obtained with $\sigma_{\rm star} = 171$ km s^{-1}, in reasonable agreement with the 141 km s^{-1} that was reported by Terlevich, Diaz, & Terlevich (1990) at their lower spectral (9 Å) and spatial (4″.9) resolutions. Star velocities obtained by direct Gaussian fits to the Ca triplet agreed well with the velocities obtained by cross-correlation and provided an independent estimate on uncertainties. The zero point of the velocity scale was verified with our spectrum of HD 101013. Within 20″ radii, we estimate our velocity uncertainties to be ± 20 km $^{-1}$.

2.3.3. *Constraints on Visual Continuum Emission from the Jet*

Dutil et al. (1995) reported excess 0.53 μm emission compared to the red along the jet in their map of continuum colors. This is not due to changes in stellar population because the "green" patch is very elongated. We note that the centroid of this emission is displaced from the active jet, which appears to lie almost NS at these radii (§ 4.4). On energetic grounds, Dutil et al. (1995) excluded optical synchrotron emission from the jet and scattered (by dust or electrons) photons from the active nucleus. They also argued that dust destruction by the jet would not deredden the background bulge sufficiently to explain the 0.53 μm excess. They suggested instead that the excess is free-free emission from hot gas that has been excited by high-velocity shocks (see also our § 4.2). If so, it should brighten slowly into the blue and dilute the equivalent widths of the stellar absorption lines along the jet compared to those elsewhere.

We see no such reduction in equivalent widths. Figure 4 compares two spectra averaged over intervals of five pixels (3″.9) that have been extracted from the long-slit spectrum before it was dereddened. One is formed on the nucleus, the other is centered 23″ to the SE. Panel *a* shows that the two spectra, when scaled to have the same flux in the near-IR continuum, also have Ca triplets with similar equivalent widths. The 10%–20% excess at 0.53 μm that was reported by Dutil et al. (1995) is obvious in panel *b*, where the levels of the two near-IR continua have been scaled to match. In panel *c*, with the red continua matched, the blue continuum at the nucleus is ≈70% larger than that 23″ to the SE. However, the equivalent widths of the blue Ca H and K lines remain the same. This is the behavior expected if dust is depleted near the nucleus. A reduction of $A_V \approx 0.4$ mag is sufficient (if $R = 3.1$) to account for the spectral difference at the nucleus. Dutil et al. (1995) felt that this effect was inadequate by itself to explain the amplitude of the blue color index in their map and argued for a contribution by free-free emission from shocked gas. Our spectrum discounts this contribution.

The incomplete spatial coverage of our slit prevented us from improving on the detection (which we now regard as a limit) of Dutil et al. (1995) for the surface brightness in the visual continuum of the jets. From our analysis and their limit, we conclude that the jets do *not* emit a continuum within the interval $\lambda\lambda = 0.38$–0.88 μm down to a surface brightness of 3×10^{-17} ergs cm^{-2} s^{-1} Å^{-1} arcsec^{-2}.

2.3.4. *Determination of the Internal Reddening and Line Fluxes*

We mapped the spatial variation of all emission-line fluxes by fitting, simultaneously to all of the obvious emission lines, Gaussians of a single width and velocity shift. In CWT, we used a 2.5 Å resolution spectrum to show that the red [S II] doublet flux ratio is in its low-density limit ($n_e < 125$ CM^{-3}) along the SE jet. In our fits we therefore imposed the constraint that both this doublet and the blue [O II] doublet be fixed at their low-density limits. The continuum level of the fits was also allowed to vary, to account for baseline tilts in the residual spectrum after starlight subtraction.

We compared the observed ratios of the Hβ/Hα line fluxes to expected values for gas in case B recombination conditions at the above density. The theoretical value depends on the dynamical state of the gas, which is reduced by collisional excitation processes. Anticipating the results of § 4.2, we used the ratio 0.34 ± 0.1 found by Sutherland, Bicknell, & Dopita (1993, hereafter SBD) from their shock models of the emitting filaments near the jet of Cen A (Morganti et al. 1991). The observed ratios average 0.25 ± 0.05 and 0.20 ± 0.05 (1 σ deviations) SE and NW of the nucleus, respectively. The implication that extinction is higher in the NW (far side) of the galaxy disk is consistent with the orientation of NGC 4258, which increases the H I column (van Albada 1980) and X-ray absorption (Pietsch et al. 1994) on the NW side. The observed

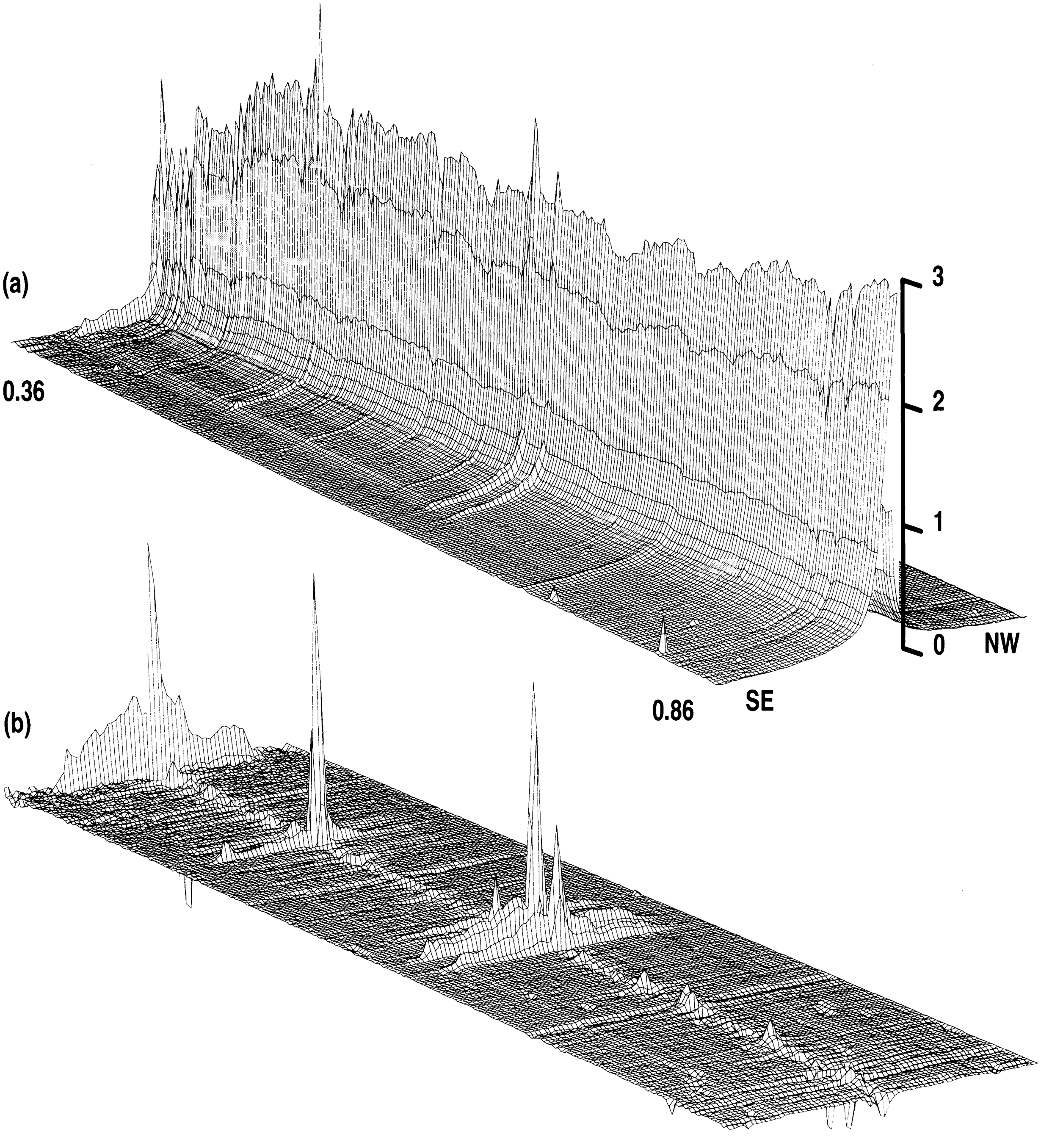

FIG. 3.—Final combined long-slit spectrum of NGC 4258 through the nucleus along P.A. 30°, after sky subtraction, but (*a*) before and (*b*) after subtraction of the galaxy continuum using a Gauss-smoothed version of the scaled nuclear spectrum of the S0 galaxy NGC 3115. The region plotted runs from (*left*) 0.36 μm to (*right*) 0.86 μm (and is linear in wavelength), and SE (foreground) to NW (background) of the galaxy nucleus out 1.′5 radii. The vertical scale in panel *a* is in units of 10^{-15} ergs cm^{-2} Å^{-1} s^{-1}; it has been magnified threefold in panel *b*

Hβ/Hα flux ratios become very small near the nucleus, even after a starlight subtraction that corrects for metal-line absorption. While harder X-rays provide evidence of a strongly absorbed active galactic nucleus (AGN) in NGC 4258 (Makishima et al. 1994), this discrepancy undoubtedly arises from differences in the Balmer-line strengths between this star-forming spiral galaxy and the S0 NGC 3115.

Line fluxes were corrected for internal extinction with the IRAF "deredden" task, which uses the reddening curve of Cardelli, Clayton, & Mathis (1989); we need on average $A_V = 1$ mag along the SE jet with $R = 3.1$ to attain the theoretical Balmer decrement. With this reddening, the ratio Hγ/Hβ = 0.39, which is still 20% too low for case B recombination whatever the temperature. None of the higher Balmer lines are

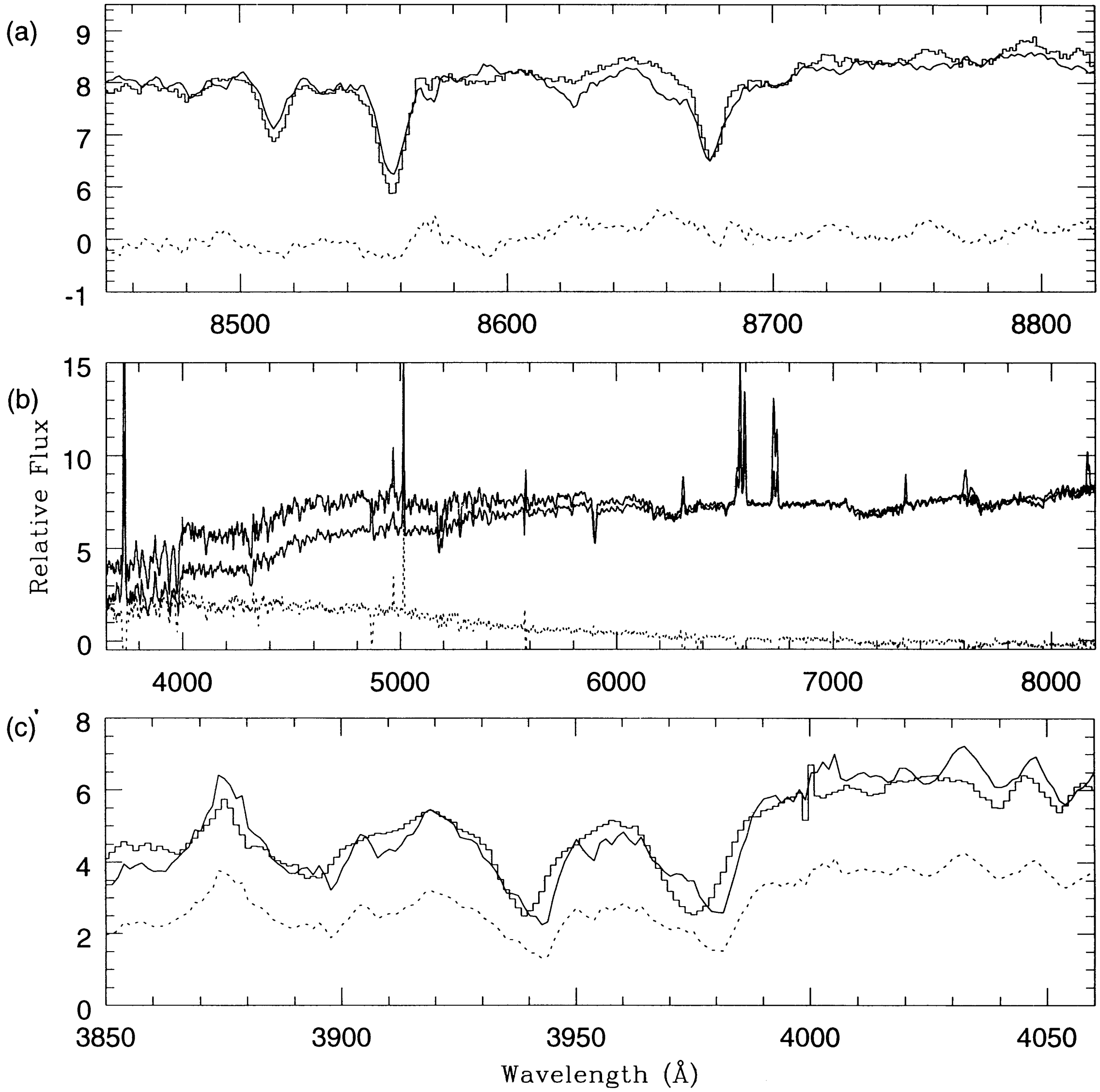

FIG. 4.—Changes in continuum slope at the nucleus. Two spectra summed over intervals of 3″.9 on the nucleus/jet (*histograms*) and 23″ SE away (*solid lines*) are compared. The off-nuclear spectrum has been boxcar smoothed slightly (to match the velocity dispersion), shifted by 2 pixels, and scaled by 14 × to match the continuum level of the nuclear spectrum. (*a*) Equivalent widths of the near-IR Ca triplet are similar for both spectra. (*b*) Comparison of the full spectra after adjusting the red continuum level. The nuclear spectrum has a stronger blue continuum. Reduced reddening on the nucleus of $A_V \approx 0.4$ magnitudes is sufficient to explain their difference, the dotted line. (*c*). Calcium H + Hϵ and K profiles at the nucleus and the profiles 23″ away, after multiplying the latter by an added factor of 1.65 × ; dotted line shows their difference before rescaling. They both have the same equivalent width, which indicates that a nonstellar continuum is *not* diluting the nuclear spectrum. The peak near 3870 Å is [Ne III].

visible in the residual spectrum. (We used the same curve and extinction to adjust the [O III], [N II], and Hα fluxes of the SE jet in our Fabry-Perot data cubes.) Figure 5 (Plate 18) plots line flux and kinematic variations along the slit.

2.3.5. *Constraints on the Fluxes of Weak Lines*

The small variations in line flux ratios that are visible in Figure 5 suggested that we sum those rows of the dereddened but not continuum-subtracted spectrum that span the SE jet from 20″–80″ radii, to better constrain the average fluxes of weak lines. Next we Gauss smoothed the summed spectrum to match the larger velocity dispersion of the nuclear spectrum of NGC 3115. The slowly varying rotation curve of the gas (Fig. 5*e*) suggests that stellar velocity dispersions are not appreciably increased by averaging along the slit. Then, following the scaling and subtraction procedure outlined by Ho, Filippenko, & Sargent (1993, hereafter HFS), we first split the spectrum of NGC 4258 into several pieces from which we then subtracted optimally scaled segments of the NGC 3115 template spectrum. Apart from a few low-frequency oscillations, noise introduced by differences in telluric water vapor absorption between 0.69–0.74 μm that was not removed by the spectrophotometric standards because of variable cirrus, the result (Fig. 6, *bottom*) satisfactorily accentuates the [Ne III] λ3869, [S II] $\lambda\lambda$4069, 4076, Hγ, [N I] λ5199, [Ar III] λ7136, and [O II] λ7325 lines. The summed, dereddened flux of each line along the SE jet relative to the flux of Hβ is listed in Table 2.

We have also detected He I λ5876 and possibly He II λ4686 emission. Limits on these and on the important auroral lines [O III] λ4363 and [N II] λ5755 also appear in Table 2. A small

1995ApJ...452..613C

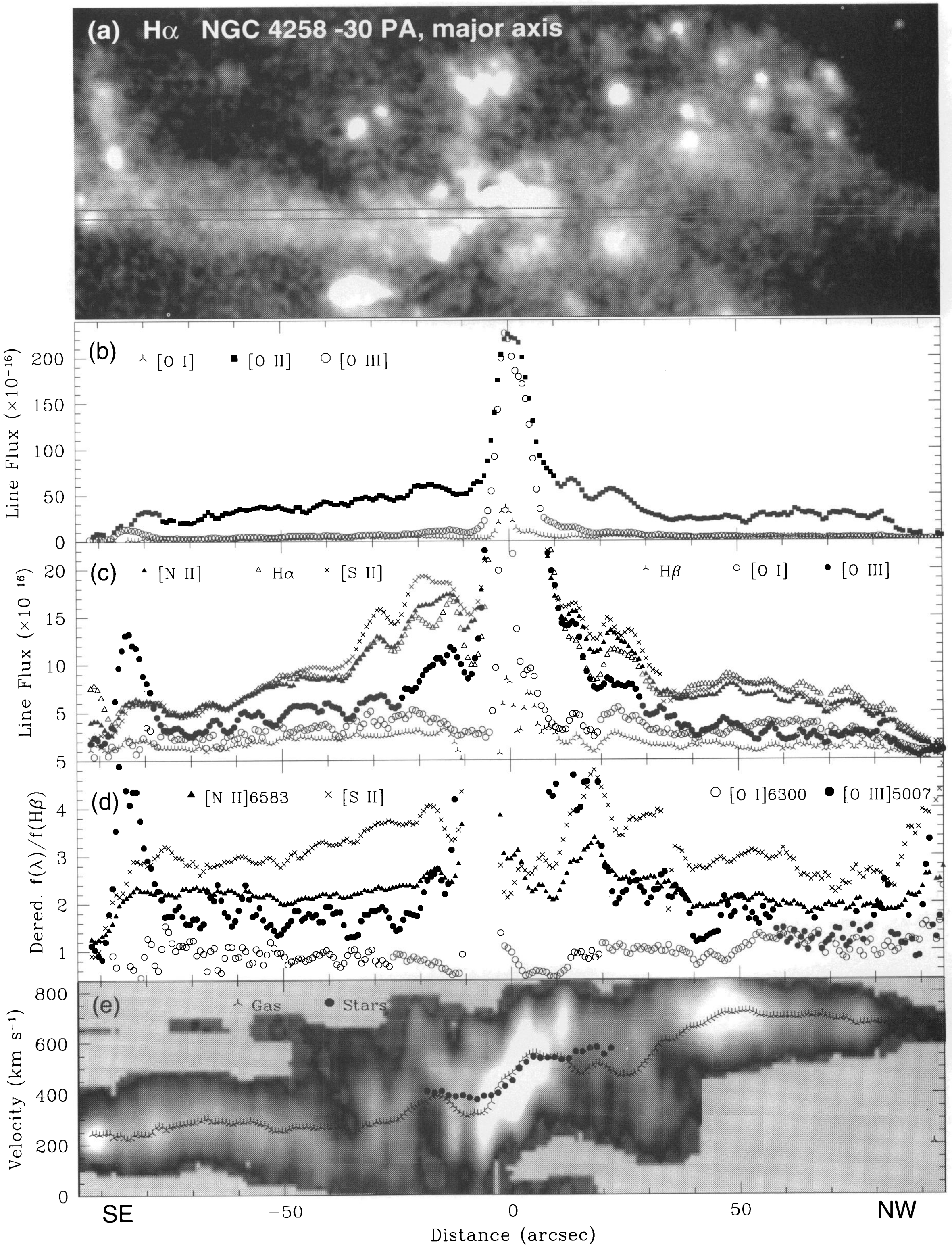

FIG. 5.—Emission-line fluxes and velocities derived from the Goldcam long-slit spectrum along P.A. −30°. (*a*) Hα image, derived from the Fabry-Perot data cube of CWT. This has been rotated so that the galaxy major axis (and jet axis) is aligned left to right. The overplotted lines show how the 2″ wide Goldcam long-slit samples the gas distribution. (*b*–*c*) Observed (not dereddened) line fluxes. (*d*) Flux ratios to Hβ, dereddened assuming case B recombination conditions at 10^4 K and a Balmer decrement of 2.9. (*e*) Gaseous and stellar velocities plotted atop a gray scale representation of the Hα profile along the galaxy major axis.

CECIL, MORSE, & VEILLEUX (see 452, 618)

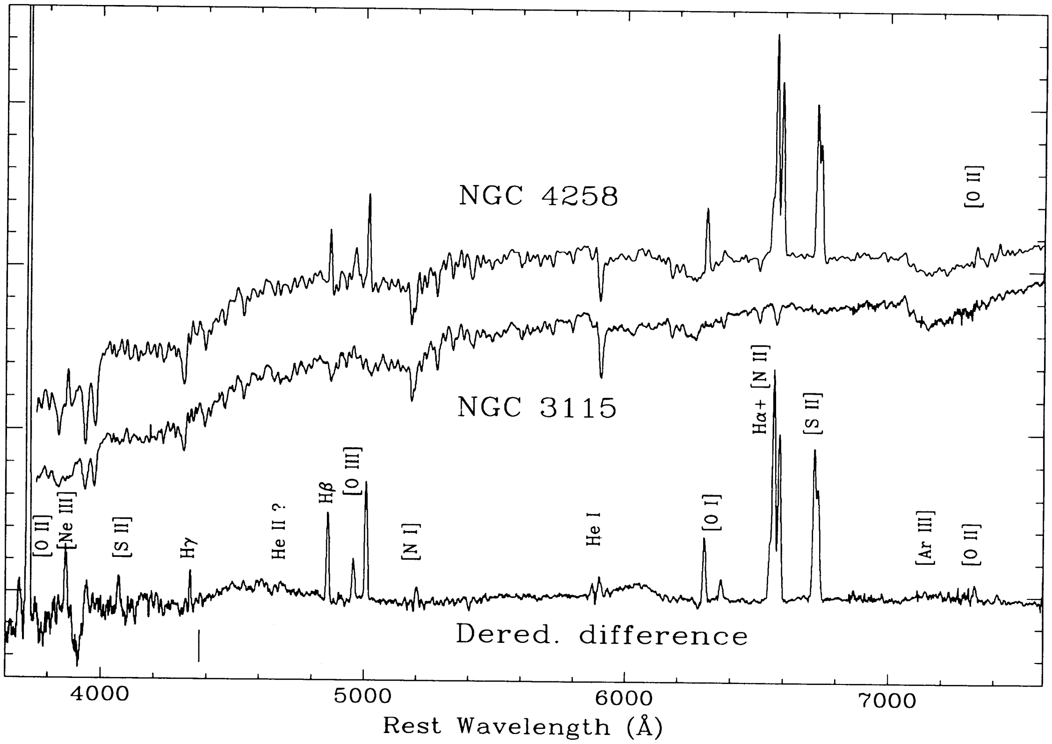

FIG. 6.—(*top*) Flux calibrated, but not dereddened average spectrum of the SE jet of NGC 4258, smoothed to the velocity dispersion of NGC 3115, and summed over 20″–80″ radii. (*middle*) Summed, flux calibrated, nuclear spectrum of the S0 galaxy NGC 3115. (*bottom*) Difference of the two spectra above, then dereddened, with emission lines marked. The [O II] λ3727 doublet extends offscale to twice the intensity shown here. The expected position of [O III] λ4363 is marked below with a vertical line. The [O II] λ7325 emission line is clearer in the top spectrum.

emission bump visible in the subtracted spectrum is offset by 2 Å from the expected position of [O III] λ4363. Because this exceeds our estimated velocity errors, we do not feel that we have detected this line. Rose & Tripicco (1984) have emphasized the danger of being led astray by spurious spectral matches when the [O III] λ4363 line is expected to have low equivalent width. Careful subtraction with different templates is required.

The referee suggested that we compare the above procedure for correcting emission-line fluxes for stellar absorption with the standard technique used for spectrophotometry of H II regions in disk galaxies. This is to add ≈1.9 Å in equivalent width of the stellar continuum (e.g., McCall, Rybski, & Shields 1985). Verification of this approach would be useful for the analysis of other optical jets when a template spectrum is unavailable. We measured line fluxes in the summed spectrum

TABLE 2

EMISSION-LINE FLUXES, LIMITS, AND FLUX RATIOS OF THE SE JET

Transition	$F(\lambda)/F(\mathrm{H}\beta)$,[a] Observed	$F(\lambda)/F(\mathrm{H}\beta)$ 20″–80″;[a] Radius, Dereddened	$F(\lambda)/F(\mathrm{H}\beta) > 80''$;[a] Radius, Dereddened
O II λ3727	16 ± 8	20 ± 10 (11)	9 ± 6
Ne III λ3869	0.45–0.52	(0.5)	...
S II λ4073	0.2–0.3	0.2–0.3 (0.3)	...
Hγ	0.2–0.3	0.22–0.33 (0.45)	...
He II λ4686	(<0.1)	(<0.1)	...
Hβ	1	1[b]	1
O III λ5007	3.1 ± 1.3 (1.4)	1.8 ± 0.2 (1.3)	2.9 ± 1.2
N I λ5199	0.1–0.2	0.12–0.17 (0.14)	...
He I λ5876	0.1	0.12	...
O I λ6300	1.2 ± 0.8	0.9 ± 0.1 (0.8)	0.3 ± 0.3
Hα	3.9 ± 0.8	2.9	2.9
N II λ6583	3.6 ± 0.7	2.2 ± 0.1 (2.0)	1.9 ± 0.4
S II λλ6717+31	3.4 ± 0.9 (4.6)	3.1 ± 0.3 (3.2)	2.2 ± 0.7
Ar III λ7136	(0.07)	(0.09)	...
O II λ7325	0.17–0.23	0.15–0.20 (0.17)	...

[a] The ± values are 1 σ standard deviations around the mean values along the slit (Fig. 5). Ranges on weaker lines reflect differing estimates of the adjacent continuum in the summed spectrum along the SE jet (Fig. 6). Ratios formed from strong lines in this spectrum are given in parentheses.

[b] Sum of dereddened Hβ flux along the SE jet in a 2″ width slit = 6.83×10^{-13} ergs s^{-1} cm^{-2}.

of NGC 4258 (Fig. 5, *top*) and applied the correction. Template subtraction leads to an Hβ flux of 2.4×10^{-13} ergs cm^{-2} s^{-1}, and in this case the correction procedure indeed yields the same value $(1.6 + 1.9 \times 0.45) \times 10^{-13}$ ergs cm^{-2} s^{-1}. Similarly, we obtain 3.4×10^{-13} and $(2.9 + 1.9 \times 0.45) = 3.8 \times 10^{-13}$ ergs cm^{-2} s^{-1}, respectively, for [O III] λ5007. The agreement between the two techniques is acceptable for this jet.

3. EMPIRICAL RESULTS

3.1. *Temperature Constraints*

At the observed low-density limit of the collisionally excited lines (CWT) we can constrain the average S$^+$, O$^+$, O^{++}, and N$^+$ temperatures by placing limits on the fluxes of the faint auroral and transauroral lines. Flux estimates of these weaker lines are uncertain because the profiles sit on a highly structured residual stellar continuum. Even when flux is detected at the nominal wavelength of the line as derived from stronger lines, the height of the adjacent continuum is often ambiguous. In addition, the red [O II] lines lie in a spectral region that is contaminated by time-variable OH emission bands. However, Figure 6 shows that we have subtracted the sky accurately enough to isolate the red [O II] and [Ar III] lines.

We used the profile of the strong [O III] λ5007 line as a template to set the height of the residual continuum below the blue [S II] λ4073 doublet. We slid the "continuum" level down the [S II] doublet profile until the line width from a Gaussian fit was 1.4 times that of the single [O III] λ4959 line (this factor was established by smoothing a simulated doublet to our derived spectral resolution). The temperature that we derive (Aller 1984) from the ratio with the red doublet fluxes, electron density $n_e \approx 10^2$ cm^{-3} (CWT), and $A_V = 1$ is $T_{\rm S^+} \leq 20{,}000$ K. Using the profile of [O I] λ6300 as the template, we obtain $T_{\rm O^+} \leq 9000$ K from the ratio [O II] λ3727/[O II] λ7325 = 65. The internal error of these two flux ratios, probably $\pm 20\%$, arises from uncertainties in the adopted reddening and continuum level. The limit $T_{\rm N^+} \leq 9000$ K is consistent with that on $T_{\rm O^+}$, but is much tighter (estimated 1 σ uncertainty of 10%) because of the comparatively strong [N II] λ6583 flux, the smaller reddening baseline, and the excellent match between the spectra of the two galaxies near 5755 Å (Fig. 6). The O^{++} temperature is only weakly constrained at less than 30,000 K because near 4363 Å, the metallicity, reddening, and perhaps stellar populations differ between the two galaxies. Figure 7 shows how scaling errors in the ratios translate into temperature uncertainties. The issue of what photoionizes the gas—shock precursor, young stars, or an AGN—is discussed in § 4.

3.2. *Variations in Gaseous Excitation*

Volume filling factors, which scale line fluxes, can be suppressed by taking ratios of collisionally excited and recombination emission lines. In this way the mean gaseous excitation can be established. The excitation of the jets can be efficiently summarized in the "diagnostic diagrams" introduced by Baldwin, Phillips, & Terlevich (1981) and subsequently compared to more data from spectral surveys by Veilleux & Osterbrock (1987) and Osterbrock, Tran, & Veilleux (1992). In the last two studies new line ratios are constructed from the fluxes of species near in wavelength, so are fairly immune to reddening errors. The diagrams clearly distinguish between AGNs and galaxies with normal H II region spectra. LINERs (Heckman 1980) plot below the AGNs in these diagrams, often with shocked galactic objects, and are mostly separated from H II regions. The separation is complete if "transition LINERs" (HFS) are excluded.

In Figure 5*d* we plot the dereddened ratios to Hβ along the locus of peak X-ray emission in the SE jet. Figure 3 shows that at radii of less than 80″ the [O III]/Hα flux ratios jump by more than 50% as the slit crosses distinct jet strands SE of the nucleus. Figures 1*f* and 5*d* show that this ratio peaks along the SE end of the jet, whereas the other line ratios do not change.

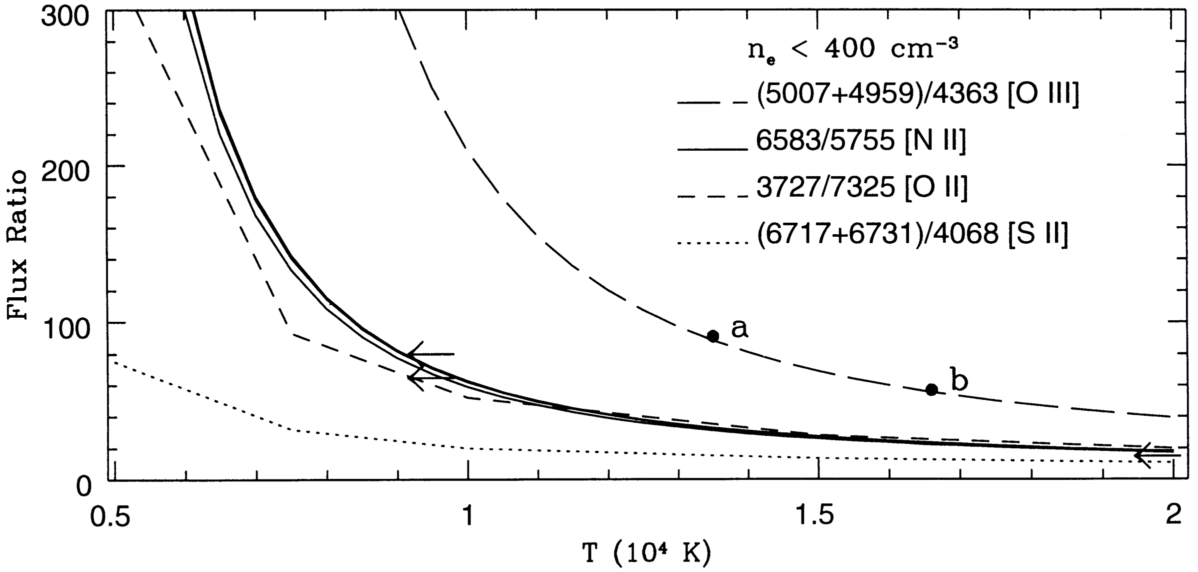

FIG. 7.—Temperature constraints derived from ratios of the indicated dereddened emission-line fluxes. The electron density is constrained by the red [S II] doublet ratio to be in the lower limit of this transition, $n_e \leq 125$ cm^{-3}, but we show the curves for the more conservative limit of 400 cm^{-3}. Uncertainties are $\approx \pm 20\%$ on the limits shown. The arrows mark our 1 σ upper limits. Points *a* and *b* label the O^{++} temperatures estimated by SBD for the models of the Cen A filaments that we use in our Table 2. These points are consistent with our weak constraint on this temperature of $<$30,000 K.

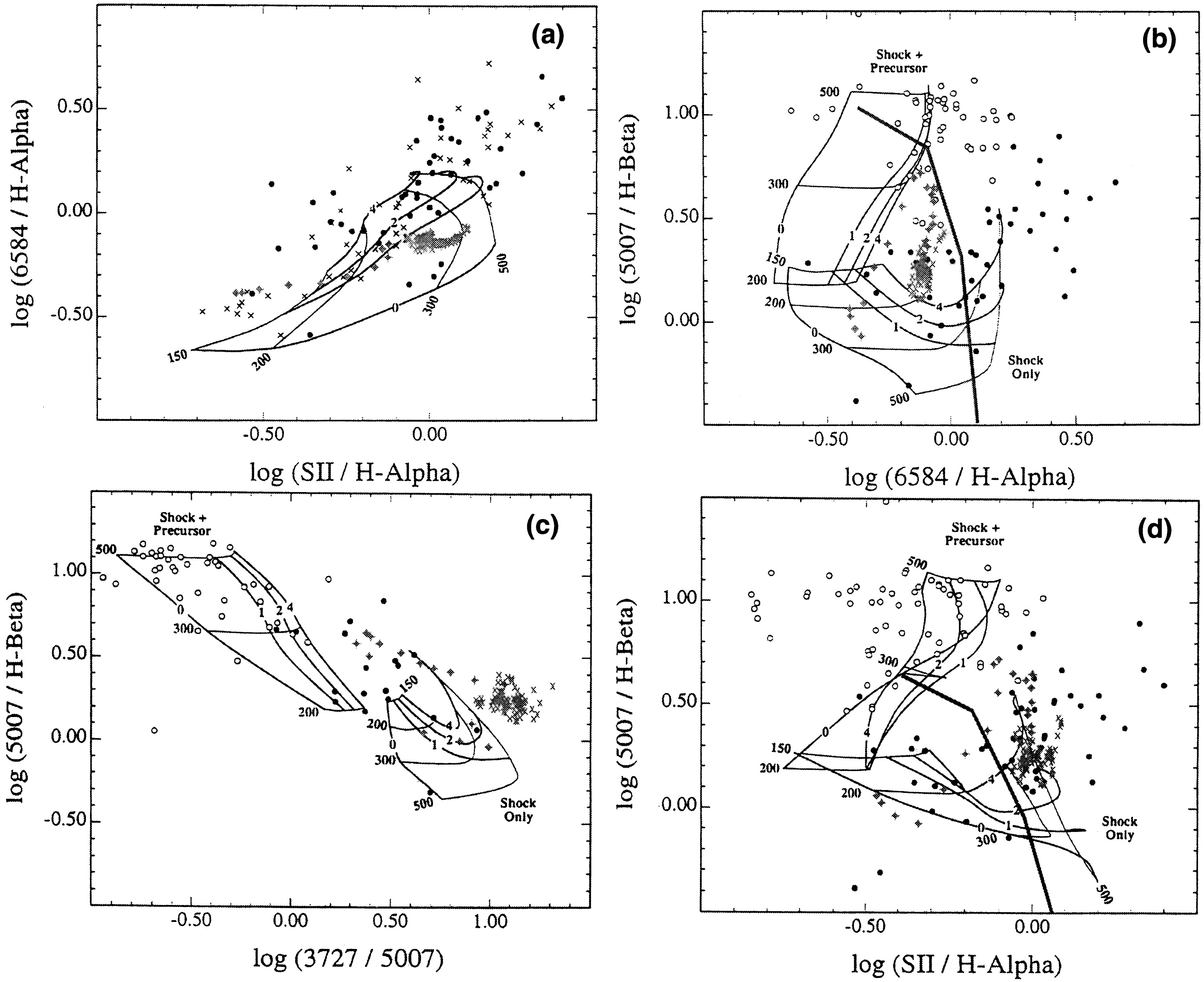

FIG. 8.—Diagnostic diagrams formed from the ratios of reddening-corrected emission lines and shock models from Dopita & Sutherland (1995b). Open circles show observations of Seyfert galaxies, dark crosses show radio galaxies, and filled circles show LINERs (see Dopita & Sutherland 1995b for references to the original data.) Most of the points for NGC 4258 plot in the LINER regime: gray crosses plot ratios at points 15″–80″ from the nucleus, while gray diamonds plot ratios from 80″ radius to the end of the jet. The theoretical grids use either the radiative "shock only," or, for the grids in panels *b–d* labeled "shock + precursor," include the H II region ahead of the shock front that is photoionized by the upstream EUV photons. The grid curves are labeled by shock velocity in units of kilometers per second and by magnetic parameter in units of μG $(n_0/1\ \mathrm{cm}^{-1})^{1/2}$. The nearly vertical gray lines summarize the single-zone photoionization models discussed by HFS, with preshock atomic density $n_0 = 10^{2.5}$ cm^{-3} and ionization parameter log U decreasing from −2.5 to −4 (*top to bottom*). Sequences for larger densities are generally parallel and to the right of the ones shown here; lower densities are inconsistent with the electron densities derived from the red [S II] doublet.

Figure 8 shows that most of the jet has LINER excitation, with points at the largest radii plotting in the H II region domain. Even the ratios with Hα of fainter lines such as [O II] λ7325 plot in the LINER domain (Osterbrock et al. 1992). From this we conclude that the compact features visible near the end of the jet (extreme left edge in Fig. 5*a*) are H II regions, while the bulk of the jet could be excited by the various candidates proposed for LINERs (which are discussed in § 4.)

3.3. *Kinematic Variations*

To check for kinematic variations between lines, we compared the results of fits where all lines were allowed to move by only a single velocity shift to those where the lines were allowed to float to their best-fit wavelengths. We found no absolute deviations greater than 0.3 pixel, ≤ 30 km s^{-1}, in the velocity-linearized summed spectrum along the jet. The one possible exception is the [O II] λλ3726, 3729 doublet, although it is very close to one end of our spectrum. This constraint on shock models will be discussed in § 4.2.3.

4. DISCUSSION

Why do the jets have LINER excitation? LINERs display a larger range of ionization than emitted by galactic H II regions, but do not show the high-ionization lines found in Seyfert nuclei. In galactic nuclei the origin of this large range has been much discussed, with emission from the low-ionization species required to come from denser, partially ionized zones that are photoionized by an almost flat near-UV continuum. The source might therefore be a dilute/heavily extinguished power-law AGN (Halpern & Steiner 1983), a thermal spectrum above 10^5 K from an accretion disk (Pequignot 1984), or the various photoionized regions that arise in shocks of several hundred km s^{-1} (Dopita & Sutherland 1995*a*). Our spectra also have $O:O^+:O^{++}$ ratios that Shields (1992) explained with normal O5 or hotter stars ($T_{\rm eff} \geq 50{,}000$ K) in a gaseous environment with composite hydrogen densities $n \geq 10^{3.5}$ cm^{-3}. In NGC 4258 there is an obscured AGN that may beam ionizing radiation along the jets (but not along our line of sight), there is plenty of hot X-ray gas with $T > 10^6$ K, the jets are supersonic and interacting strongly with adjacent molecular gas so secondary shocks from thermal instabilities are certain, and the jet may trigger star formation by compressing the adjacent molecular clouds. Evidently and in common with LINERs as a class (see, e.g., HFS 1993), the extranuclear LINER spectrum along the jets of NGC 4258 could arise from any or all of the mechanisms mentioned above. We now consider each in turn.

4.1. *Role of the Active Nucleus*

A subparsec diameter disk, with major axis of 87° that is almost perpendicular to the radio jet at smallest radii, was revealed in the VLBA observations of water vapor masers by Greenhill et al. (1995 and references therein). This disk is slightly warped and shows Keplerian motion around a mass of 3.6×10^7 $M_\odot$ within a radius of less than 0.13 pc (Miyoshi et al. 1995). This suggests that jet emission could be excited by hard photons that escape from the AGN along the polar axis of the nuclear disk.

The AGN is evident as a weak broad component of the nuclear Hα profile (Keel 1983; Filippenko & Sargent 1985). It is probably also responsible for the X-ray Fe K-line emission of equivalent width 0.25 ± 0.10 keV seen by *ASCA* (Makishima et al. 1994). In addition, Stüwe et al. (1992) found from their spectra that the velocity-integrated Hα flux halves from the nucleus to $R = 1''$. They fitted line ratios for $R \leq 5''$ with photoionization models of spectral form $F_\nu \propto \nu^\alpha$ and $\alpha = -1.2$. The strongly absorbed ($\log N_{\rm H} \approx 23.2$ cm^{-2}) AGN, with $\alpha \approx -1.8$ and $L_{2-10\,\rm keV} \approx 2.4 \times 10^{40}$ erg s^{-1}, was subsequently uncovered by Makishima et al. (1994) with the *ASCA* X-ray spectrometers. These authors note that the inferred flux of hydrogen-ionizing photons ($\approx 2 \times 10^{51}$ s^{-1}) can account for the emission near the nucleus. Our Figures 3 and 5*b* show that the emission is sharply peaked on the nucleus and changes its form of excitation away (e.g., the flux ratio [O II] λ3727/Hβ becomes very strong). Our observations support the view of Stüwe et al. (1992) that the nuclear region is directly photoionized by the attenuated AGN.

Does the AGN also directly excite the gas along the jet? This often appears to happen in Seyfert galaxies with "ionization cones" (e.g., Wilson & Tsvetanov 1994). Dutil et al. (1995) considered the role of scattered nuclear flux to explain their observation of 0.53 μm emission from the jet. They found that dust or electron scattering of AGN light failed by several orders of magnitude to explain this continuum emission. We can employ the following photon balance argument to argue against significant excitation of the emission lines by the nucleus. Figure 1 shows that the end of the SE jet spans different angular sectors when viewed in [N II] and [O III]. Seen from the nucleus, the brightest part of the [O III] arc would span at least 23° or 51° if the arc lies in the sky plane or in the large-scale disk of NGC 4258 (which is inclined to our line of sight by ≈70°; CWT), respectively. The bright arc would be displaced ≈24–50°, respectively, from the spin axis of the nuclear disk. This suggests an opening angle to the nuclear radiation of up to 100°, consistent with values deduced for ionization cones in other active galaxies (Wilson & Tsvetanov 1994) and with the thinness of the disk as measured by Miyoshi et al. (1995). The (assumed planar) arcs would then be expected to intercept $\ll 1\%$ of the current nuclear flux of $\approx 2 \times 10^{51}$ s^{-1} hydrogen-ionizing photons (Makishima et al. 1994), if this flux is emitted isotropically. The total Hα emission of the SE jet after dereddening is at least 4.4×10^{39} ergs s^{-1} (CWD), requiring 1.5×10^{51} s^{-1} ionizing photons during a typical recombination time of $10^5/n_e \gtrsim 10^3$ years if case B conditions hold. Because the jets cover only a small solid angle as seen from the nucleus, for them to be directly photoionized the AGN must have been 10^3 times more luminous within the past thousand years, and currently be in a low state. This is unlikely because the near constancy of the observed ionization parameter down the SE jet (Fig. 8) would then require a fortuitous match between the R^{-2} decline in gas densities required to compensate for geometric dilution and the R^{-1} density gradient required to maintain constant U with a recently faded central source.

Is the gaseous excitation of the rest of the SE jet consistent with ionization from the nucleus? Stüwe et al. (1992) interpreted their spectra with photoionization models and preferred hot (O6) stars as the exciting sources from 1″ radius out to 100″. Possible ionization from hot stars along the jet will be discussed in § 4.3. The straight gray line segments in two panels in Figure 8 summarize sequences of single-density cloud models computed by HFS with Ferland's (1991) CLOUDY photoionization code. For the most part, the sequence for hydrogen density $n \leq 10^4$ cm^{-3} (corresponding to ionization fractions $\geq 1\%$) is consistent with our data if the ionization parameter in their single-density approximation log $U \leq -3.5$. However, the observed [O II]/[O III] flux ratio is twice that predicted by HFS for the same model sequence. The tendency for the radiation field to harden off the jet at large radii (gray diamond symbols in Fig. 8) would be explained in this scenario by an increase in U as the hydrogen number density drops either with radius or because the gas lifts out of the disk plane at larger radii, or by hardening of the radiation field from absorption by the abundant molecular gas (e.g., Krause et al. 1990) at smaller radii. Another explanation is given in the next section.

4.2. *Shocks along the Jets*

Evidence for shock excitation of this gas was presented in CWD, and can be summarized as follows. The *ROSAT* HRI shows that most of the X-ray–emitting gas lies along the jets, while the spatially averaged PSPC spectrum of the jets is consistent with a thermal origin. When the observed spectrum is fitted assuming collisional equilibrium, its temperature $kT = 0.3 \pm 0.05$ keV. This peak temperature is attained behind a shock of 500 km s^{-1}, although the gas is then not in collisional equilibrium. Nonequilibrium cooling may be evident because the fit is imperfect at high energies even when the nuclear region is excluded. If the emission arises from entrainment, we also expect a range of shock velocities. The highest velocities would arise from gas near the jet but those velocities responsible for the visual-band lines would come from dense, slower filaments that are torn by Kelvin-Helmholtz instabilities (e.g., SBD). In any event, the velocity inferred from the thermal X-ray spectrum is consistent with the ± 325 km s^{-1} excursions around the local mean velocity that are seen in the emission-line profiles within 30″ radius SE of the nucleus (CWT).

Dutil et al. (1995) argued that they could account for the color change that they mapped near the nucleus with a combination of dust destruction within the jet and free-free emission from a 450 km s^{-1} shock with a plausible density of the preshocked gas. However, as discussed in § 2.3.3, the spectrum near the nucleus does not show a dilution of absorption-line equivalent widths that is expected for significant nonstellar emission, so free-free emission has not been observed. The limit on surface brightness given in § 2.3.3 does not usefully constrain shock models.

For preshock atomic density n_0 cm^{-3}, shock area A_6 kpc^2, and shock velocity V_{200} in units of 200 km s^{-1}, the Hα luminosity of the shock plus its photoionized (by the shock) precursor is

$$L_{\mathrm{H}\alpha} = 2 \times 10^{39} n_0 V_{200}^{2.32} A_6 \text{ ergs s}^{-1} \tag{1}$$

(Dopita & Sutherland 1995*a*.) The luminosity is halved if no precursor is present. For the three-strand SE jet, CWT estimated an area of $A_6 = 2.4$, which leads to a modest atomic density within the ambient medium of $n_0 \lesssim 0.1(0.2)$ cm^{-3} for a $\geq$400 km s^{-1} shock with (without) a photoionized precursor. This density should be produced easily by the observed molecular gas in the galaxy disk (e.g., Krause et al. 1990), so the shocks might be locally photoionizing the gas and therefore not require anisotropic emission from the AGN.

Stüwe et al. (1992) also considered and dismissed shock excitation of the jets because the line ratios did not agree with published shock models. However, Dopita & Sutherland (1995a, b) have recently produced new models which show that the LINER regime in diagnostic plots can also be fully spanned by a few parameters, principally shock velocity V_s ranging from 150 to 450 km s^{-1}, a magnetic field parameter $Bn^{-1/2}$ ranging over 0–4 μG cm$^{3/2}$, and the presence or absence of emission from the photoionized shock precursor. That such velocities (CWT) and fields (30 μG, albeit in the nonthermal particles; Hummel, Krause, & Lesch 1989) are seen along the jets of NGC 4258 is further circumstantial evidence for shocks. The strong X-ray emission from the jets (CWD) shows that all of the postshock photons are not being absorbed by the ambient gas, so models without precursors are favored for NGC 4258. The net radiation field has smaller U without a precursor (Dopita & Sutherland 1995a, b).

In Figure 8 we overplot the model predictions of Dopita & Sutherland (1995b) for the line ratios that arise from shocks of different pairs of (V_s, B). Usually our measured ratios along the jet cluster in the shock-only regime near $V_s \approx 300$ km s^{-1}, despite the monotonic decrease of emission-line widths beyond 50″ (Fig. 5*e*). An exception is seen in Figure 8*c*, where the dereddened [O II] fluxes appear to be too large by 0.25 dex. However, this is just the average reddening correction derived from the hydrogen lines. The models of Sutherland, Bicknell, & Dopita (1993) show that the [O II] emission can come from a different region, plausibly with almost no reddening.

Unlike in many other LINERS, we do not need to posit an ad hoc nitrogen enhancement above solar abundance to obtain good agreement with the models (see Dopita & Sutherland 1995b, § 4.2.) This is consistent with the observations of Zaritsky, Kennicutt, & Huchra (1994), who find solar oxygen abundances in the H II regions across the inner disk of NGC 4258. From these plots we also see no evidence for collisional deexcitation of ratios involving [S II]. This is consistent with the postshock gas being in the low-density limit, plausibly because compression has been inhibited by magnetic support. Finally, we note that points at larger radii (gray diamonds in Fig. 5) trend from the LINER toward the Seyfert regime in the diagnostic diagrams. Dopita & Sutherland (1995b) interpret points in the latter as arising from a combined shock + precursor radiation field. Buildup of a precursor is very plausible at larger radii in NGC 4258.

Shock models predict correlations between the amplitude of the emission-line velocity oscillations and the gaseous excitation, an effect not produced by anisotropic nuclear beaming. We do not find this effect along the SE jet of NGC 4258. There are at least two ways for the shock interpretation to survive in the face of this decoupling of observed kinematics and gaseous excitation. First, we could posit that the line widths decrease because the flow twists sharply and decreases its motion along the line of sight. This is plausible, as shown in Figure 5*a* (shown even better in Fig. 11 of CWT), which shows that the Hα strands that are tightly coiled closer to the nucleus diverge beyond 50″ radius. A second, less contrived, explanation follows from the recognition by SBD that species of different excitation are emitted from distinct regions within the shocked flows that have different physical conditions. One would then argue that the constant line ratios reflect the continued presence of the region that preferentially emits these lines, but with differing filling factors along the jet.

A further indication that shocks are responsible for the LINER-like excitation along the SE jet would be to derive similar values of V_s and B from each excitation diagram. Comparing the model grids of Dopita & Sutherland (1995b) to our data in the excitation diagrams (Fig. 8) we see that the points do tend to cluster in similar small regions of most of these diagrams, which suggests almost constant physical conditions.

4.2.1. *Assumptions for Shock Models*

To interpret the dispersion in dereddened flux ratios as physical changes within the gas, we tried to reproduce the ratios with shock models similar to those used by SBD in their study of the ionized jet of Cen A. Unlike SBD, we have a plausible lower limit on the shock velocity from the observed velocity oscillations. This value suggests that when the SE jet coils tightly near the nucleus, we sometimes see much of the intrinsic gas motion. Moreover, in CWT we presented evidence that the shocks in NGC 4258 are locally photoionizing the gas. This means that we might not have the ambiguity of Cen A, where gaseous ionization may be controlled by a "blazar beam" from the AGN, rather than locally by shocks. (SBD note that the two excitation modes can in principle be distinguished by measuring resonance line strengths in FUV spectra, but such observations have not yet been made with the *HST* FOS.)

All models that successfully reproduce galaxy LINER spectra require stratified regions at different gas density (e.g., Pequinot 1984; Shields 1992) to emit the different line species. In the scenario of SBD, two gas clumps of unequal density collide to drive two shocks into each other. It is likely that this occurs in NGC 4258 because the light jets are colliding with the dense molecular ISM (Martin et al. 1989; Krause et al. 1990; Plante et al. 1991). The density difference leads to different shock speeds and therefore to different peak temperatures, which yield different ionization fields on the shock precursors to alter the structures of the shocks. The observed emission-line spectrum comes from the precursor and cooling postshock gas, weighted by their relative volumes and emissivity in the different wavebands. Low- and high-ionization species are emitted mostly from the dense secondary and more rarefied fast shocks, respectively. The low-ionization lines have volume-weighted temperatures below 10^4 K and the other lines come from gas with $T > 15{,}000$ K. The relative prominence of the highly ionized to less ionized species increases as the radiation field from the fast shock more strongly heats the ambient, precursor ISM.

The models of SBD depend on the following parameters (with appropriate values for NGC 4258 in parentheses): chemical abundances (assumed to be closely solar following the study of Zaritsky et al. [1994] from 18 H II regions), cloud density contrast (limited by SBD to 10:1 for computational reasons), preshock density in the tenuous component of the precursor ISM (taken to be ≤ 1 cm^{-3} from CWD's estimate of the X-ray surface brightness along the SE jet), shock area (assumed to be 2.2×10^6 pc^2 from CWD's assumption that three jet strands are responsible for all of the X-ray emission SE of the nucleus), and the velocities of the two shock systems. In the less dense gas, the shock velocity is constrained from CWT to be ≥ 325 km s^{-1} near the nucleus and concentrated CO emission, and ≈ 50 km s^{-1} beyond $\approx 50''$ down the SE jet away from the CO gas. The velocity of the secondary shock in the dense CO gas is more problematic because only interferometer arrays have sufficient spatial resolution to isolate this gas along the jets, but kinematics have been established only for the molecular gas associated with the jet NW of the nucleus (Plante et al. 1991). While these data clearly show interactions between the NW jet and adjacent ISM, that jet is apparently redirected at many Hα hot spots, which prevents us from usefully constraining the space motion of the associated emission-line gas.

SBD also show that the emission spectrum depends on the degree to which the shocked flow fragments. In one-dimensional models (Innes 1992, and references therein) the flow fragments when shock velocities exceed ≈ 100 km s^{-1}, but SBD expect physical flows to instead flatten into sheets. The degree of fragmentation in the cool gas behind the slow shock affects the efficiency with which radiation is absorbed by gas ahead of this shock. In a completely fragmented flow, dense, thermally collapsed blobs absorb little of the radiation and so have small partially ionized zones with little emission from low-ionization species. The main precursor is highly ionized and prominent if there is sufficient gas ahead of the shock. If the flow remains mostly smooth, the downstream radiation is efficiently absorbed and lines from low-ionization species are prominent.

4.2.2. *Comparison with the Data*

In Table 3 we compare our dereddened line ratios with those computed by SBD and a new set graciously computed for us by M. A. Dopita using a recent (1995 February) version of the MAPPINGS II code introduced by Sutherland & Dopita (1992). We will discuss a more comprehensive set of shock models in a future paper. Figure 8 shows that our data are more consistent with shock models that do not include the precursor. In NGC 4258, the precursor is apparently density bounded because we do see the X-rays that it did not absorb. Models *a* and *b* in Table 3 include a precursor, but models *c* do not. Models *a* and *b* set magnetic field parameter $B = 0$, but models *c* have $B = 4\mu\mathrm{G}/(n_0/1\ \mathrm{cm}^{-3})^{1/2}$. For the most part, this model range spans our data except that the observed [O II]/Hβ ratio, even before dereddening, is more than twice the predicted value. SBD find that most of the N^+ and O^+ emission comes from dense filaments that were compressed by the secondary shock in the dense medium and ionized by the fast shock. For the parameters selected in their Cen A study, this gas is cooler than 8000 K, a temperature consistent with the values or limits that we derive from our observed line ratios (§ 3.1).

4.2.3. *Possible Kinematic Differences between Emitting Zones*

The SBD models produce most [O II] λ3727 emission from the dense secondary shock. This shock should propagate at velocity $v_2 = v_1(n_1/n_2)^{1/2}$ compared to the fast, X-ray–emitting shock. If we attribute the observed ±325 km s^{-1} oscillations around the mean gas motion to gas that has passed through the fast shock, we would expect the [O II] λ3727 doublet to show oscillations of reduced amplitude. In our summed spectrum along the jet we would expect slightly reduced line widths for the deblended [O II] doublet compared to the other lines. In particular, from fits to the Hβ and [O III] profiles we would expect each of the [O II] lines to have a dispersion of 3.5 pixels. Instead, the blended doublet is best fitted with the lines constrained to be in the ratio appropriate for the low-density limit if each width is 3.9 pixels. As discussed in § 3.3, the doublet is shifted by at most 50 km s^{-1} compared with the other lines, which is larger than the ≈ ±10 km s^{-1} linearization residuals that we estimate across our combined spectrum. However, the blue [O II] doublet is at one end of our spectrum, so it seems prudent to assign somewhat larger uncertainties there. We conclude that we have a tentative detection of kinematic differences between the shock zones, but we require more sensitive

1995ApJ...452..613C

TABLE 3

OBSERVED RATIOS OR THEIR LIMITS VERSUS MODELS OF PHOTOIONIZING SHOCKS

TRANSITION	$F(\lambda)/F(\mathrm{H}\beta)$ DEREDDENED	MODEL *a* 250 km s^{-1}	MODEL *b* (km s^{-1})		MODEL *c* (km s^{-1})		
			300	450	150.0	300.0	450.0
O ii λ3727	20 ± 10	4.1	5.3	6.4	6.8	10.4	13.7
Ne iii λ3869	(0.5)	0.3	0.3	0.4	0.32	0.68	1.18
O iii λ4363	(<0.06)	0.06	0.09	0.10	0.19	0.08	0.07
He ii λ4686	(<0.10)	0.07	0.07	0.11	0.05	0.15	0.27
O iii λ5007	1.8 ± 0.2	3.5	3.6	3.4	1.91	1.57	3.31
N ii λ5755	(<0.02)	...	...	...	0.03	0.04	0.07
He i λ5876	(0.15 ± 0.05)	...	...	...	0.07	0.17	0.16
O i λ6300	0.9 ± 0.1	1.2	1.2	1.5	0.36	2.14	3.21
Hα	2.9	(3.0)	(3.0)	(2.9)	3.07	2.94	2.97
N ii λ6583	2.2 ± 0.1	1.8	1.9	2.8	1.54	3.84	4.66
S ii $\lambda\lambda$6717+31	3.1 ± 0.3	3.6	3.4	3.3	1.52	2.48	2.55
O ii λ7325	(0.10 ± 0.04)	...	...	...	0.05	0.16	0.08

NOTES—Model *a*: Two equal-density colliding shocks, smooth postshock flows, optically thin precursors, $n_0 = 1$ cm^{-3}, $B = 0$. Model *b*: 10:1 density contrast between two colliding shocks, fragmented postshock flows, optically thin precursors, $n_0 = 1$ cm^{-3}, $B = 0$. Model *c*: Single shock model with $n_0 = 1$ and $B = 4\mu\mathrm{G}/(n_0/1\ \mathrm{cm}^{-1})^{1/2}$ and no precursor emission.

spectra with a shorter wavelength limit to confirm the kinematic differences expected to arise in multiple shocks.

4.3. *Jet-induced Star Formation*

The jet is flowing in the disk, so it might induce the dense cool gas to collapse and form stars. This process has been much invoked to explain the "alignment effect" at high redshifts (see, e.g., McCarthy 1993) and may have actually been seen in Minkowski's object (van Breugel et al. 1985). Unfortunately, the theoretical development (see, e.g., de Young 1989) is too vague to predict the mass spectrum of formed stars, so the efficiency by which the unprocessed ISM is ionized is unknown.

Stüwe et al. (1992) argued from photoionization models of their spectra of NGC 4258 that the outer ≈80% of the jets are ionized by adjacent O6 stars. Energy requirements are a modest one star per ≈100 pc, on average. Shields (1992) has shown that hotter stars (O5, $T_{\mathrm{eff}} = 50{,}000$ K) can generate a LINER spectrum. However, his predicted line ratios differ from our observed values, probably because the low-ionization lines have been collisionally deexcited at the high densities (10^5 cm^{-3}) required in his models. In CWD we estimated that the SE jet must entrain $\approx 6\ M_\odot\ \mathrm{yr}^{-1}$ to be shock excited along its 2.5 kpc length (in agreement with the estimate of Martin et al. 1989). Therefore, as the O(30) O6 stars form from adjacent molecular clouds, the jet would entrain O(10^6) $M_\odot$ to produce O(10^3) $M_\odot$ just in the most luminous stars. Any plausible IMF (which current models of jet/ISM interactions do not constrain) will increase the mass formed in stars at least tenfold.

Unfortunately, as Stüwe et al. (1992) point out, these stars are probably mostly obscured along our line of sight by molecular gas, so they may be invisible even to *HST*. However, if still embedded in molecular gas, they should be strong sources of reprocessed infrared photons. The total 10 μm luminosity within a radius of 3″ is $4 \times 10^7\ L_\odot$ (Cizdziel, Wynn-Williams, & Becklin 1985), but unfortunately IR emission along the jets is currently unconstrained. Lacking constraints on ionizing stars, we consider less massive stars. Rose (1985) has shown that the ratio of the central intensity of the combined Ca ii H and Hϵ absorption to that of Ca ii K is a good discriminant between a population of F, G, and K stars (where it is constant), and A and B stars where the Ca ii lines weaken and Hϵ strengthens. To within the uncertainties introduced by emission-line contaminants, the two spectra in Figure 4*b* indicate similar stellar populations. We therefore find no evidence from the visual spectrum that the circumnuclear region of NGC 4258 has undergone recent formation of massive stars.

A long-slit spectrum of the nuclear region along P.A. −30° was kindly acquired for us by D. DePoy in early June of 1995, using the OSIRIS spectrometer with a 4″ wide slit, and NICMOS array on the Perkins 1.8 m telescope at Lowell Observatory. Preliminary analysis in a 4″ × 10″ box shows a faint H_2 line one-third the intensity of Brγ, on a strong continuum and an unusually deep CO absorption. The latter result is consistent with millimeter observations (Martin et al. 1989; Krause et al. 1990; Plante et al. 1991). We will discuss the IR spectrum in a forthcoming paper (Cecil & DePoy, in preparation.)

4.4. *Recent Nuclear Activity*

As we noted in CWD, the disk discussed by Greenhill et al. (1995) is perpendicular to the radio jet from the smallest detectable radius out to at least 2500 light years SE of the nucleus. In CWD we used a high-resolution 6 cm image from the VLA archive to tentatively identify a bright region in [N ii] and Hα at ≈1 kpc radius as the current head of the linear jet. Figure 1*d* labels this point, which the other panels show appears to have the gaseous excitation of an H ii region. Courtès et al. (1993) have cataloged the Hα fluxes and derived total luminosities for many H ii regions in the disk of NGC 4258. Our candidate for the jet head is their complex No. 51, which they find has total $L = 33{,}000\ L_\odot$ uncorrected for reddening. If the jet propagates at 0.1*c*, this extent suggests that the collimation geometry at small radius has had a fixed orientation for at least the last 25,000 yr. More probably, for jet speed V_{jet}, the head advances at a rate $V_{\mathrm{head}} = \eta^{1/2} V_{\mathrm{jet}}/(1 + \eta^{1/2})$ with η the density contrast between light jet fluid and dense ambient medium (Norman et al. 1981). The advance time to the putative head of the active jet is then probably more like 10^6 yr.

We constrained the most recent jet activity with a 35 minute A-array exposure at 20 cm from the VLA archive. This image (insert in Fig. 2) shows a NS extension out to a radius of 2″ (70 pc) that is perpendicular to the nuclear disk and indicates outflow within the last 20,000 yr.

5. SUMMARY

Our multifrequency observations of these jets are very naturally interpreted within the framework of high-velocity radiative shocks, as developed recently by Dopita & Sutherland (1995a, b). In balance, we favor shock excitation of the jet gas because it reproduces: the visual emission-line spectrum, the ± 325 km s^{-1} oscillations in the emission-line profiles that are consistent with the postshock temperatures derived from the thermal spectrum of X-ray emitting gas that is tightly aligned with the jets, and the Hα luminosity of the jets with modest ambient densities that are readily available in fragments torn from the adjacent molecular clouds. We have shown that recent models of shocks with velocities consistent with the X-ray temperature do not violate our observed values or limits on the temperatures of several ionized species and predict the observed line ratios along the jets.

If the "jets" are not photoionized locally, they must instead be almost static, fossil structures at radii greater than 3 kpc. One must then accept that they are directly photoionized by either young stars along the boundary of the molecular clouds perhaps induced to form by the jet compression, or by anisotropic emission from the AGN. The first process does not explain the soft X-rays or kinematic oscillations. The second is probably inconsistent with the constancy of the ionization parameter along the jets and requires that the nucleus has faded a thousandfold within the last thousand years.

Further observations can be made to better constrain a more complete shock treatment. Deep filtered images of the jets with high spatial resolution may resolve the region of entrainment. The possible presence of secondary shocks and jet-induced star formation in the adjacent molecular gas can be constrained with long-slit IR spectrophotometry. Higher resolution VLA images can be made to further constrain spectral indices and the distribution of relativistic particles along the jets. X-ray spectrometers before AXAF do not have the combination of angular and spectral resolutions required to reliably isolate the complex thermal spectrum of the jets from hard X-ray disk and nuclear sources. NGC 4258 remains a choice target for more sensitive X-ray spectroscopy than reported in CWD and Pietsch et al. (1994).

Ultraviolet spectra will probably be required to firmly establish the source of excitation along the jets. Models (see, e.g., SBD) show that the fluxes of important resonance cooling lines are far higher for shock heated than directly photoionized gas. Unfortunately, the large extent that makes the jets of NGC 4258 rewarding targets for ground-based study makes such observations prohibitively time consuming with the current single-aperture spectrometers on *HST*.

We used radio maps generously provided by P. Crane and S. Caganoff or extracted from the VLA archive. We thank Diane Harmer for obtaining the 1994 spectra during KPNO service observing, and the referee for very useful comments. G. C. thanks NSF (AST 90-22128) and NASA (NAG 5-2347) for grants to the University of North Carolina, Russel Cannon, and Joss Hawthorne for the hospitality of the Anglo-Australian Observatory where this paper was started, and Michael Dopita and Ralph Sutherland for their model results before publication. J. M. was supported by NASA grants NAGW-2689 and NAGW-3268 awarded to A. Wilson at the Space Telescope Science Institute. S. V. was supported by NASA through grant number HF-1039.01-92A awarded by the Space Telescope Science Institute which is operated by the AURA, Inc., for NASA under contract No. NAS 5-26555.

REFERENCES

Aller, L. H. 1984, Physics of Thermal Gaseous Nebulae (Boston: Reidel)
Baldwin, J. A., Phillips, M. M., & Terlevich, R. 1981, PASP, 93, 5 (BPT)
Bland, J., & Tully, R. B. 1989, AJ, 98, 723
Bland-Hawthorn, J., Shopbell, P., & Veilleux, S. 1995, in preparation
Cardelli, J. A., Clayton, G. C., & Mathis, J. S. 1989, ApJ, 345, 245
Cecil, G., Bland, J., & Tully, R. B. 1990, ApJ, 355, 70
Cecil, G., Wilson, A. S., & De Pree, C. 1995, ApJ, 440, 181 (CWD)
Cecil, G., Wilson, A. S., & Tully, R. B. 1992, ApJ, 390, 365 (CWT)
Cizdziel, P. J., Wynn-Williams, C. G., & Becklin, E. E. 1985, AJ, 90, 731
Courtès, G., & Cruvellier, P. 1961, CR Acad. Sci. Paris, 253, 218
Courtès, G., et al. 1993, A&A, 268, 419
de Young, D. 1989, ApJ, 342, L59
Dettmar, R.-J., & Koribalski, B. 1990, A&A, 240, L5
Dopita, M. A., & Sutherland, R. S. 1995a, ApJ, submitted
———. 1995b, ApJ, submitted
Dutil, Y., Beauchamp, D., & Roy, J.-R. 1995, ApJ, submitted
Ferland, G. J. 1991, Ohio State Univ. Internal Rep. 91-01 (Columbus: Ohio State Univ., Dept. of Astronomy)
Filippenko, A. V., & Sargent, W. L. W. 1985, ApJS, 57, 503
Ford, H. C., Dahari, O., Jacoby, G. H., Crane, P. C., & Ciardullo, R. 1986, ApJ, 311, L7
Goodrich, R., & Veilleux, S. 1988, PASP, 100, 1572
Greenhill, L., et al. 1995, ApJ, 440, 619
Halpern, J., & Steiner, J. E. 1983, ApJ, 269, 637
Heckman, T. 1980, A&A, 87, 142
Ho, L. C., Filippenko, A. V., & Sargent, W. L. W. 1993, ApJ, 417, 63 (HFS)
Hummel, E., Krause, M., & Lesch, H. 1989, A & A, 211, 266
Innes, D. E. 1992, A&A, 256, 660
Keel, W. 1983, ApJ, 269, 466
Krause, M., Cox, P., Garcia-Barretto, J. A., & Downes, D. 1990, A&A, 233, L1
Makishima, K., et al. 1994, PASJ, 46, L77
Martin, P., Roy, J.-R., Noreau, L., & Lo, K. Y. 1989, ApJ, 345, 707
McCall, M., Rybski, P. M., & Shields, G. A. 1985, ApJS, 57, 1
McCarthy, P. 1993, ARA&A, 31, 639
Miyoshi, M., et al. 1995, Nature, 373, 127
Morganti, R., et al. 1991, MNRAS, 249, 91
Norman, M. L., Smarr, L. L., Wilson, J. R., & Smith, M. D. 1981, ApJ, 247, 52
Osterbrock, D. E., Tran, H. D., & Veilleux, S. 1992, ApJS, 389, 196
Pequinot, D. 1984, A&A, 131, 159
Pietsch, W., Vogler, A., Kahabka, P., Jain, A., & Klein, U. 1994, A&A, 284, 386
Plante, R., Handa, T., & Lo, K. Y. 1994, in IAU Colloq. 140, Astronomy with Millimeter and Submillimeter Wave Interferometry, ed. M. Ishiguro & W. M. Welch (San Francisco: ASP), 361
Plante, R. L., Lo, K.Y., Roy, J.-R., Martin, P., & Noreau, L. 1991, ApJ, 381, 110
Rose, J. 1985, AJ, 90, 1927
Rose, J., & Tripicco, M. J. 1984, ApJ, 285, 55
Rubin, V. C., & Graham, J. A. 1990, ApJ, 362, L5
Shields, J. 1992, ApJ, 399, L27
Stone, R. P. S. 1977, ApJ, 218, 767
Stüwe, J. A., Schulz, H., & Hühnermann, H. 1992, A&A, 261, 382
Sutherland, R. S., Bicknell, G. V., & Dopita, M. A. 1993, ApJ, 414, 510 (SBD)
Sutherland, R. S., & Dopita, M. A. 1992, ApJS, 88, 253
———. 1980, A&A, 90, 123
van Albada, G. D., & van der Hulst, J. M. 1982, A&A, 115, 263
van Breugel, W. J. M., Filippenko, A. V., Heckman, T., M., & Miley, G. K. 1985, ApJ, 293, 83
van der Kruit, P. C. 1974, ApJ, 192, 1
van der Kruit, P. C., Oort, J. H., & Mathewson, D. S. 1972, A&A, 21, 169
Veilleux, S., & Osterbrock, D. 1987, ApJS, 63, 295
Wilson, A. S., & Tsvetanov, Z. 1994, AJ, 107, 1227
Zaritsky, D., Kennicutt, R. C., & Huchra, J. P. 1994, ApJ, 420, 87